Atmospheric
Measurement
Techniques
Open Access

Discussions

Design and characterization of a smog chamber for studying gas-phase chemical mechanisms and aerosol chemistry

X. Wang[1], T. Liu[1,2], F. Bernard[1], X. Ding[1], S. Wen[1], Y. Zhang[1,2], Z. Zhang[1,2], Q. He[1,2], S. Lü[1,2], J. Chen[3], S. Saunders[4], and J. Yu[5]

[1]State Key Laboratory of Organic Geochemistry, Guangzhou Institute of Geochemistry, Chinese Academy of Sciences, Guangzhou 510640, China
[2]University of Chinese Academy of Sciences, Beijing 100049, China
[3]Shanghai Key Laboratory of Atmospheric Particle Pollution and Prevention (LAP3), Department of Environmental Science & Engineering, Fudan University, Shanghai 200433, China
[4]School of Chemistry and Biochemistry, The University of Western Australia, Crawley WA 6009, Australia
[5]Department of Chemistry, Hong Kong University of Science and Technology, Kowloon, Hong Kong, China

Title Page

Abstract	Introduction
Conclusions	References
Tables	Figures

|◄ | ►|
◄ | ►

Back | Close

Full Screen / Esc

Printer-friendly Version

Interactive Discussion

AMTD

6, 7735–7769, 2013

Design and characterization of a smog chamber

X. Wang et al.

Title Page

Abstract | Introduction

Conclusions | References

Tables | Figures

|◀ | ▶|

◀ | ▶

Back | Close

Full Screen / Esc

Printer-friendly Version

Interactive Discussion

Abstract

We describe here characterization of a new state-of-the-art smog chamber facility for studying atmospheric gas phase and aerosol chemistry. The chamber consists of a $30\,m^3$ fluorinated ethylene propylene (FEP) Teflon film reactor suspended in a temperature-controlled enclosure equipped with two banks of black lamps as the light source. Temperature can be set in the range from $-10\,°C$ to $40\,°C$ at accuracy of $\pm 1\,°C$ as measured by eight temperature sensors inside the enclosure and one just inside the reactor. Matrix air can be purified with NMHCs $< 0.5\,ppb$, $NO_x/O_3/carbonyls < 1\,ppb$ and particles $< 1\,cm^{-3}$. The photolysis rate of NO_2 is adjustable between 0–$0.49\,min^{-1}$. At $298\,K$ under dry conditions, the average wall loss rates of NO, NO_2 and O_3 were measured to be $1.41 \times 10^{-4}\,min^{-1}$, $1.39 \times 10^{-4}\,min^{-1}$ and $1.31 \times 10^{-4}\,min^{-1}$, respectively; and the particle number wall loss rate to be $0.17\,h^{-1}$. Auxiliary mechanisms of this chamber are determined and included in the Master Chemical Mechanism to evaluate and model propene-NO_x-air irradiation experiments. The results indicate that this new smog chamber can provide high quality data for mechanism evaluation. Results of α-pinene dark ozonolysis experiments revealed SOA yields comparable to those from other chamber studies, and the two-product model gives a good fit for the yield data obtained in this work. Characterization experiments demonstrate that our GIG-CAS smog chamber facility can be used to provide valuable data for gas-phase mechanisms and aerosol chemistry.

1 Introduction

Smog chambers provide a controlled environment to study the formation and the evolution of specific compounds of interest by isolating the influence of emissions, meteorology and mixing effects. Smog chambers were initially constructed for developing and evaluating atmospheric gas phase chemical mechanisms or models for predicting secondary pollutants (Akimoto et al., 1979; Carter et al., 1982; Jeffries et al., 1982,

1985). In the mid-1980s, Seinfeld and coworkers developed a $65\,\text{m}^3$ outdoor chamber made of FEP Teflon film to study the aerosol formation from gas phase precursors such as aromatic and biogenic hydrocarbons (Leone et al., 1985; Stern et al., 1987). In the subsequent three decades outdoor and indoor chambers have been widely used to
5 study formation of secondary pollutants such as ozone (Hess et al., 1992; Simonaitis et al., 1997; Carter, 2000; Dodge, 2000) and secondary organic aerosols (SOA) (Odum et al., 1996, 1997; Griffin et al., 1999; Martín-Reviejo and Wirtz, 2005; Paulsen et al., 2005; Rollins et al., 2009), and evolution of SOA (Donahue et al., 2012).

   Chamber wall effects are known to be an important source of uncertainties when
10 evaluating the mechanisms or models (Carter et al., 1982; Carter and Lurmann, 1991; Dodge, 2000). Large volume reactors can minimize the wall loss of gas phase species and particles, therefore many studies of SOA formation have been carried out in large outdoor chambers (Leone et al., 1985; Stern et al., 1987; Pandis et al., 1991; Johnson et al., 2004; Martín-Reviejo and Wirtz, 2005; Rollins et al., 2009). But diurnal varia-
15 tions of the actinic flux and temperature make it difficult to model the experimental data and to reproduce the experiments. Considering these concerns, Cocker et al. (2001a) developed dual $28\,\text{m}^3$ indoor chambers to study the mechanisms of aerosol forma-tion. Recently, to minimize reactor effects in the studies of volatile organic compounds (VOCs) reactivity and SOA formation, Carter et al. (2005) constructed a state-of-the-art
20 indoor chamber facility with two collapsible $90\,\text{m}^3$ FEP Teflon film reactors.

   In China, some small volume smog chambers have been developed to study gas phase kinetic mechanisms since 1980s (Wang et al., 1995; Ren et al., 2005; Xu et al., 2006). Wu et al. (2007) constructed a $2\,\text{m}^3$ precisely temperature-controlled indoor smog chamber made of FEP Teflon film to study the SOA formation. However, the
25 small volumes of these smog chambers impart the disadvantage of relatively large wall effects and also make it difficult to do experiments of long duration. At present, ozone and fine particles ($PM_{2.5}$) has become serious air quality problems in China (Chan and Yao, 2008; Q. Zhang et al., 2012). As ozone and a large portion of $PM_{2.5}$ components are secondary from gaseous precursors under atmospheric gas-phase and/or multi-

Design and characterization of a smog chamber

X. Wang et al.

Title Page

Abstract	Introduction
Conclusions	References
Tables	Figures

◄ | ►►

◄ | ►

Back | Close

Full Screen / Esc

Printer-friendly Version

Interactive Discussion

X. Wang et al.

phase processes, it is imperatively necessary to set up more quality smog chambers in China for the deep understanding of complex air pollution, particularly in China's megacities.

This paper describes a new state-of-the-art indoor smog chamber facility established in Guangzhou Institute of Geochemistry, Chinese Academy Sciences (GIG-CAS). This GIG-CAS chamber facility is designed to study formation mechanisms of ozone and SOA as well as evolution of SOA, to evaluate the mechanisms under low NO_x and VOCs conditions, and to serve as a platform for evaluating the performance of newly developed gas or particle monitors. A series of initial characterization experiments have been carried out and are discussed in this paper.

2   Facility

The 8.5 m × 4.0 m × 3.5 m thermally insulated enclosure is housed in a 14.0 m × 6.0 m × 8.5 m laboratory in the first floor has been equipped with an array of continuous gas phase and aerosol phase monitors. Situated directly over the enclosure on the second floor are off-line VOCs/semi-VOCs/ions/anions samplers and analyzers. The list of equipment is shown in Table 1. Inside the enclosure are a 30 m^3 reactor made of FEP Teflon film (FEP 100, Type 200A, DuPont, USA) with dimensions of 5.0 m × 3.0 m × 2.0 m and two banks of 60 W 1.22 m black lamps. A schematic of the GIG-CAS smog chamber is shown in Fig. 1a.

2.1   Enclosure

The inner walls of the enclosure are covered with reflective and polished stainless steel sheets to obtain a maximum and homogenous light intensity. The floor is covered with less reflective but more durable stainless steel sheets. The enclosure temperature is controlled by three cooling units (total power 40 KW), which are located outside the laboratory next to the enclosure. The cooling air is distributed uniformly and constantly

in three different ducts through the enclosure false ceiling made of perforated reflective aluminum sheets, and is returned to the cooling units through a porous high efficient 3.0 m × 0.2 m × 0.6 m filter that contains activated charcoal inside to clean the enclosure air. A heater is also installed inside each duct. Eight thermocouples (Fig. 1a) are placed approximately 1 m above the housing floor between the enclosure and the reactor walls. The enclosure temperature is controlled by an electronic control system through adjusting the power of cooling units and heaters according to the difference between the average temperature of the eight thermocouples and the set temperature.

2.2 Teflon reactor

The reactor wall material is 2 mil (54 μm) FEP Teflon film that is transparent, chemically inert and UV permeable. The Teflon film is flexible enough to avoid altering the pressure inside the reactor during air extraction. The Teflon reactor is made by a heat sealing laminator. All seams on the reactor are reinforced by a polyester film tape with a silicone adhesive (Polyester Tape 8403, 3M, USA). The reactor wall is more than 1 m away from the lights to avoid the heating on the surface of the Teflon film. The reactor is mounted inside the enclosure with a fixed bottom stainless steel frame and a movable top stainless steel frame. The top frame is lifted and lowered by a mechanical step motor which has power-off protection. During experiments, as the volume decreases due to sampling, leaks and permeation, the top frame is lowered slowly to maintain a differential positive pressure between the inside of the reactor and the enclosure, thereby reduce the contamination of the enclosure air. Siemens QBM 66.201 (Siemens AG, Germany) is used to measure the differential pressure between the reactor and the enclosure with an accuracy of ±3 Pa. When the reactor volume decreases to 1/3 of its maximum value, the experiment (typically about 10 h, depending on the numbers of instruments taking samples from the chamber) will be terminated.

Four Teflon ports are installed inside the reactor. One port located in the middle of the chamber floor has 12 holes of 0.635 cm in diameter. This port is used for injection of purified air, sample and seed aerosols. A second port next to the instruments, with

13 holes of 0.635 cm in diameter, is used for sampling. The other two ports, each with 4 holes of 0.635 cm in diameter, are also used for sampling. Besides, an air blower is connected to the reactor through a 10 cm solenoid valve controlled by computer, providing a pumping flow rate of 1 $m^3 min^{-1}$.

Two 3-wing stainless steel fans coated with Teflon are installed at the bottom inside the reactor to provide sufficient mixing of the gas species and particles. No detectable non-methane hydrocarbons (NMHCs) are emitted from the fans. Rotating speed of the fans can be varied to a maximum of 1400 rpm by adjusting the input power.

2.3 Light source

A total of 135 black lamps (1.2 m-long, 60 W Philips/10R BL, Royal Dutch Philips Electronics Ltd, the Netherlands) are arranged in two banks as the light source. One bank of 80 lamps are mounted on one enclosure wall, and another bank of 55 lamps are mounted near the opposite enclosure wall on an aluminum alloy frame. The artificial light produced by the black lamps gives a good representation of the ground-level solar light spectrum in the low wavelength region, but they do not emit in the longer wavelength regions (> 400 nm) which photolyze some organic compounds such as methylglyoxal in the range of 450–550 nm (Cocker et al., 2001a). However, because of the low-cost and efficient UV irradiation, black lamps are frequently used in environment chamber experiments (Cocker et al., 2001a; Carter et al., 2005; Hynes et al., 2005; Wu et al., 2007). The 135 black lamps are divided into 4 separately controlled groups; therefore the light intensity can be regulated to different levels.

2.4 Air purification system

As matrix gas for simulation experiments and carrier gas for reactants, purified dry air is supplied by passing compressed house air through a condenser and Thermo Zero Air Supply (Model 1160, Thermo Scientific, USA). The maximum flow rate of purified air is 45 L min^{-1}. The purified dry air includes < 0.5 ppb NMHCs, < 1 ppb NO$_x$, O$_3$ and

Title Page

Abstract | Introduction

Conclusions | References

Tables | Figures

◄ | ►|

◄ | ►

Back | Close

Full Screen / Esc

Printer-friendly Version

Interactive Discussion

carbonyl compounds, and no detectable particles. A separate source of purified air with < 5 ppb NMHCs (mainly ethane and propane) is also used for high concentration precursors (hundreds of ppb) experiments. This source of purified air is obtained by forcing compressed house air with a maximum $200\,L\,min^{-1}$ through a combustion chamber filled with Hopcalite and a series of bed scrubbers filled with activated charcoal, Purafil, Hopcalite, allochroic silica gel, and a PTFE filter. The schematic of these two air purification systems is shown in Fig. 1b.

Before each experiment the reactor is evacuated and filled with purified dry air for at least 5 times, then the reactor is flushed with purified dry air at a flow rate of $100\,L\,min^{-1}$ for at least 48 h. After cleaning, no residual hydrocarbons, O_3, NO_x, or particles are detected in the reactor. When the reactor is not in use, it is continuously flushed with purified dry air.

2.5 Injection system

Gaseous reactants are injected using gas-tight syringes through a septum installed in one port of a union tee which is connected in a FEP Teflon line, and then flushed by purified dry air or nitrogen into the reactor. For the introduction of liquid reactants, known volumes are measured and injected by microliter syringes through a heating system with an injection port similar to that of gas chromatography. Ozone is generated by a commercial ozone generator (VMUS-4, Azco Industries Ltd, Canada) with pure oxygen as the feed gas to prevent from generating NO_x. Ozone introduced into the reactor is controlled by the generating time and the flow rate.

Humidification is achieved by vaporizing Milli-Q ultrapure water contained in a 0.5 L Florence flask and the water vapor is flushed with purified dry air into the reactor. Relative humidity inside the reactor can be varied from $< 5\%$ to 80%. The humidification process does not introduce detectable hydrocarbons or particles into the reactor.

Seed particles are generated by an atomizer (ATM-220, Topas GmbH, Germany) and pass through a diffusion dryer (DDU-570, Topas GmbH, Germany) to remove water

Design and characterization of a smog chamber

X. Wang et al.

and a neutralizer (TSI 3080, TSI Incorporated, USA) to eliminate the charge before introducing into the reactor.

2.6 Instrumentation

The array of gas phase and aerosol phase instruments equipped with the chamber facility is briefly described in Table 1.

Ozone is measured by an EC9810 ozone analyser (Ecotech, Australia), which is calibrated weekly using a Thermo Scientific Model 146i multi-gas calibrator. The detection limit and accuracy of the ozone instrument are 0.5 ppb and ±0.5 %, respectively. An EC9841T chemiluminiscence analyzer (Ecotech, Australia) is used to measure NO and NO_2. The NO_x instrument is calibrated weekly using a certified cylinder of NO. The detection limit and accuracy of the NO_x instrument are 50 ppt and ±0.5 %, respectively.

VOCs inside the reactor are measured both offline and online. Off-line measurement are performed by using a Mode 7100 Preconcentrator (Entech Instruments Inc., USA) coupled with an Agilent 5973N gas chromatography-mass selective detector/flame ionization detector/electron capture detector (GC-MSD/FID/ECD, Agilent Technologies, USA). During simulation air inside the reactor are sampled about every 15 min with evacuated 2 L stainless steel canisters, and analyzed using the off-line analysis system for a wide spectrum of VOCs. This analytical system has been well established and detail description of the method can be found elsewhere (Wang and Wu, 2008; Y. L. Zhang et al., 2010, 2012, 2013). Carbonyl compounds are analyzed off-line by high performance liquid chromatography (HPLC, HP1200, Agilent Technologies, USA) coupled to UV detection at 360 nm after collected by drawing air through a Sep-Pak DNPH-Silica Cartridge (Waters Corporation, USA) with a sampling pump (Thomas, USA) every 15 min. Detail description of the method can be found elsewhere (Tang et al., 2003).

Online monitoring of parent NMHCs such as propene, α-pinene, and some aromatic hydrocarbons and their oxidation products are also available with a proton-transfer-reaction time-of-flight mass spectrometer (PTR-TOF-MS, Ionicon Analytik GmbH,

Austria). Detailed descriptions of the PTR-TOF-MS technique can be found elsewhere (Lindinger et al., 1998; Jordan et al., 2009). At present the accuracies for some species by the PTR-TOF-MS are still not comparable to that by offline methods, e.g., PTR-MS quantification of HCHO is highly influenced by the humidity (Vlasenko et al., 2010). Therefore in this work we only report our VOCs results by offline techniques, and further calibration of the PTR-TOF-MS is still under way.

Particle number concentrations and size distributions are obtained using a Scanning Mobility Particle Sizer equipped with a Differential Mobility Analyzer (TSI 3081, TSI Incorporated, USA) and a Condensation Particle Counter (TSI 3775, TSI Incorporated, USA). Flow rates of sheath and aerosol flow are 3.0 and $0.3\,L\,min^{-1}$, respectively, allowing a size distribution scanning ranging from 14 nm to 700 nm within 135 s. The accuracy of the particle number concentration is ±10 %.

A high-resolution time-of-flight aerosol mass spectrometer (HR-TOF-MS, Aerodyne Research Incorporated, USA) is used to measure the chemical compositions and evolutions of submicron aerosols (PM_1) (Jayne et al., 2000; DeCarlo et al., 2006). The HR-TOF-MS is also able to determine the average element ratios of organics, like H/C, O/C, and N/C (DeCarlo et al., 2006). The instrument is operated in the high sensitivity V-mode and high resolution W-mode alternatively. The HR-TOF-MS is calibrated using 300 nm monodisperse ammonia nitrate particles.

3 Characterization

3.1 Temperature control and its homogeneity

In the GIG-CAS chamber, three temperature control units and two Teflon-coated fans are used to provide a homogeneous and stable temperature inside the reactor. Figure 2a shows evolutions of the average temperatures as measured by the eight thermocouples (T1-T8, Fig. 1a) and the temperature inside the reactor (T_r, Fig. 1b) measured by Siemens QFM2160 (Siemens AG, Germany) under black light irradiation

when temperatures were setting to 40 °C, 15 °C and −10 °C, respectively. After the initial increasing or decreasing, the average temperatures got stabilized after about 1.5 h, 20 min and 40 min when the temperatures were set to 40 °C, 15 °C and −10 °C, respectively. The standard deviations of the nine temperatures were all within ±1 °C, indicating a good homogeneity of the temperature inside the enclosure and the reactor.

The average values of T_1 to T_8 and T_r at a set temperature of 25 °C under black light irradiation are shown in Fig. 2b. The experiment duration time was 6 h. All of the eight thermocouples show stable temperatures around 25 °C with accuracies within ±1 °C. Temperature inside the reactor is stable at 25.2 ± 0.5 °C during the experiment. All the subsequent experiments were carried out at a set temperature of 25 °C with a relative humidity less than 10 %.

3.2 Mixing

Ozone is chosen as a tracer to test the gas phase mixing time inside the reactor. The injection line was in the middle of the reactor near a fan. Ozone was generated at a rate of 0.8 L min^{-1} for 10 s and was injected into the reactor in three pulses. The fan rotating speed was fixed at 700 rpm. As showed in Fig. 3, ozone can be well mixed in about 120 s after each injection. Compared to the experiments duration which may be several hours, this mixing time is very short.

3.3 Dilution

Dilution may occur due to small leaks or high volume sampling. Dilution rate may vary with the number and type of instruments taking samples from the reactor. In each experiment, a low reactive compound such as SF_6 or CH_3CN was injected as a tracer for dilution. Dilution was not detectable within the uncertainty of the instrument.

3.4 Light spectrum and intensity

The light spectrum emitted by black lamps is measured by EPP2000CXR-50 Concave Grating spectrometer (StellarNet Inc, USA) and is shown in Fig. 4. The black lamps produce an irradiation over the range from 340 to 400 nm with peak intensity at 369 nm. For the wavelength above 400 nm, essentially no intensity is produced except some small peaks. In the first 8 months of operation, no appreciable variation of the light spectrum was observed.

Light intensity is represented by the photolysis rate of NO_2 which is estimated by a steady-state actinometry. The operation process includes injecting NO_2 into the reactor, irradiating it and continuously measuring the concentrations of NO, NO_2 and O_3. The photolysis rate of NO_2, J_{NO_2}, is estimated according to the equation:

$$J_{NO_2} = K_{NO+O_3}[NO][O_3]/[NO_2] \tag{1}$$

where [NO], [O_3] and [NO_2] represent concentrations (molecule cm^{-3}) and K_{NO+O_3} (Atkinson et al., 2004) is the rate constant of ozone and NO reaction. A series of NO_2 actinometry experiments were carried out. A NO_2 photolysis rate of 0.49 ± 0.01 min^{-1} at full light intensity was obtained (corrected for the reaction of ozone and NO in the sampling lines). This value is a little lower than 0.58 min^{-1} calculated by TUV/NCAR model for Guangzhou on 22 June at noon. The four separately controlled groups of black lamps allow the NO_2 photolysis rate to be varied from 0 to 0.49 min^{-1}.

3.5 Wall loss of gases

Chamber wall effects include offgasing of NO_x and other reactive species, chamber radical sources, and gases loss to the walls (Carter et al., 1982). They may have an impact on gas phase reactivity and secondary organic aerosol formation. In early times of smog chambers, Grosjean (1985) has done a series of experiments to evaluate the wall loss rates of inorganic and organic species.

In the GIG-CAS smog chamber, wall loss rates of NO, NO_2, O_3 and propene were evaluated by injecting a certain concentration of these gases and continuous monitoring their decay in the dark. Wall loss rates are obtained by treating the wall loss as a first-order process. The average wall loss rates of NO, NO_2 and O_3 were $1.41 \times 10^{-4}\,\mathrm{min}^{-1}$, $1.39 \times 10^{-4}\,\mathrm{min}^{-1}$ and $1.31 \times 10^{-4}\,\mathrm{min}^{-1}$, respectively. They are all within the range of values reported for other chamber facilities (Table 2). For propene, Wu et al. (2007) calculated a wall loss rate of $1.1 \times 10^{-7}\,\mathrm{s}^{-1}$ in a $2\,\mathrm{m}^3$ Teflon smog chamber. While in our GIG-CAS smog chamber, no wall loss of propene was observed within the uncertainty of GC-FID.

3.6 Particle wall loss

Particle deposition onto the wall of the reactor is believed to be influenced by diffusion and the charged wall. Particle wall loss rate is proportional to the particle concentration and depends on the particle size. The particle number-weighted wall loss rate is described by first-order kinetics as

$$\frac{\mathrm{d}N(d_p, t)}{\mathrm{d}t} = -K_N(d_p)N(d_p, t) \tag{2}$$

where $N(d_p, t)$ is the particle number concentration, d_p is the diameter of the particle and $K_N(d_p)$ is the particle number loss coefficient (Cocker et al., 2001a). The $K_N(d_p)$ values can be estimated from the particle number concentration vs. time data in any experiment when no new particle is formed.

Ammonium sulfate $((NH_4)_2SO_4$, AS) seed particles are introduced into the reactor to evaluate the production of water soluble inorganic particles and the particle number wall loss. $0.5\,\mathrm{mol\,L}^{-1}$ AS solution was atomized with a flow rate of $4\,\mathrm{L\,min}^{-1}$ for 20 min. As shown in Fig. 5, AS aerosols exhibit a medium diameter of 150 nm within a few minutes after the injection and the medium diameter slowly grows up to 200 nm. Values of K_N for 15–730 nm particles range from 0.08 to $0.23\,\mathrm{h}^{-1}$ in our GIG-CAS chamber.

Design and characterization of a smog chamber

X. Wang et al.

Title Page

Abstract	Introduction
Conclusions	References
Tables	Figures

◄◄   ►►

◄   ►

Back   Close

Full Screen / Esc

Printer-friendly Version

Interactive Discussion

The particle number wall loss rate is determined to be $0.17\,h^{-1}$, which means a life-time of 5.9 h for particles. The result is comparable to results reported for other smog chambers (Table 3).

3.7 Propene-NO$_x$ experiments

The propene-NO$_x$ irradiation system was widely used as a reference system (Carter et al., 2005; Hynes et al., 2005) to evaluate the ability of a chamber to test the mechanisms for single organic-NO$_x$ irradiation systems. A set of four propene-NO$_x$ irradiation runs were carried out under dry conditions with a controlled temperature of $298.3 \pm 0.5\,K$. The initial experimental conditions are listed in Table 4. The initial propene concentrations varied from 669 ppb to 967 ppb and the initial propene/NO$_x$ ratios ranged from 1.8 to 2.6.

A near-explicit mechanism for propene from the Master Chemical Mechanism version 3.2 (Saunders et al., 2003) was used to simulate the propene-NO$_x$ irradiation experiments. Auxiliary mechanisms and relevant parameters used in the model are listed in Table 5. The parameters were determined by simulating clean air, low NO$_x$-air, CO-NO$_x$-air and CO-air irradiation experiments. Reaction rate coefficients of the N$_2$O$_5$ hydrolysis to adsorbed HNO$_3$, the photolysis of adsorbed HNO$_3$ to OH and NO$_2$, and the wall loss of HNO$_3$ were assumed similar to those used by Hynes et al. (2005). The reaction rate coefficient of NO$_2$ dark heterogeneous reaction NO$_2 \rightarrow 0.5$HONO$+0.5w$HNO$_3$ was determined to be $2.32 \times 10^{-6}\,s^{-1}$ from NO$_2$ dark decay experiments. As mentioned above, the ozone and NO wall loss rates were determined to be $2.19 \times 10^{-6}\,s^{-1}$ ($1.31 \times 10^{-4}\,min^{-1}$) and $2.34 \times 10^{-6}\,s^{-1}$ ($1.41 \times 10^{-4}\,min^{-1}$), respectively. The reaction rate coefficients of light-induced production of OH and offgasing of NO$_2$ from Teflon walls (Carter and Lurmann, 1991; Bloss et al., 2005) were determined to be $0.005J_{NO_2}$ by simulating the experiments. The initial HONO concentration was varied from 0 to 5 ppb to give best fits to the experimental concentration profiles.

Figure 6 shows a comparison of observed and simulated concentration-time profiles of a propene-NO_x irradiation system. The initial HONO concentration was adjusted to be 5 ppb to give the best fit for this experiment. Good agreements are obtained for most of the compounds such as propene, O_3, NO, HCHO and CH_3CHO. The model shows a faster sink for NO_2 in the last one hour. O_3 is over-predicted at the end of the experiment with a relative deviation of 4.8 %. The quantity $\Delta([O_3] - [NO])$ is used to evaluate the model performance (Carter et al., 2005; Pinho et al., 2006). This quantity is defined as:

$$\Delta([O_3] - [NO]) = [O_3]_{final} - [NO]_{final} - ([O_3]_0 - [NO]_0) \tag{3}$$

where $[NO]_0$, $[O_3]_0$, and $[NO]_{final}$, $[O_3]_{final}$ are the concentrations of NO and O_3 at the beginning of the experiment, and at the end, respectively. $\Delta([O_3] - [NO])$ represents the amounts of NO oxidized and O_3 formed in the experiments, and also gives an indication of the biases in simulating O_3 formation. In the four experiments, the prediction biases of $\Delta([O_3] - [NO])$ are calculated to be varied from −2.2 % to 23.7 % at the end of the experiments, which are within the values of ±25 % reported by Carter et al. (2005) when simulating VOC-NO_x systems. The model results mentioned above illustrate that the GIG-CAS smog chamber can provide valuable data for mechanism evaluation.

3.8 α-pinene ozonolysis SOA yield

A series of experiments of α-pinene ozonolysis in the dark were carried out to evaluate the chamber facility in studying SOA formation chemistry. This reaction has been widely studied and numerous data are readily found in the literature (Hoffmann et al., 1997; Griffin et al., 1999; Cocker et al., 2001b; Saathoff et al., 2009; Wang et al., 2011). Methods developed by Pankow (1994a, b) and Odum et al. (1996) are used to analyze the data. Briefly, SOA yield, Y, is defined as follows:

$$Y = \frac{\Delta M_0}{\Delta ROG} \tag{4}$$

where ΔROG is the mass concentration of reactive organic gas (ROG) reacted, and ΔM is the total mass concentration of organic aerosols formed. Y is a function of M_0 and the relation is described as:

$$Y = M_0 \sum \left(\frac{\alpha_i K_{om,i}}{1 + K_{om,i} M_0} \right) \qquad (5)$$

where $K_{om,i}$ and α_i are the mass-based absorption equilibrium partitioning coefficient and stoichiometric coefficient of product i, respectively; M_0 is the total mass concentration of organic material. Odum et al. (1996) found that a two-product model could well fit the yield data if appropriate values for α_1, α_2, $K_{om,1}$, $K_{om,2}$ were chosen.

Five experiments of dark ozonolysis of α-pinene were carried out under dry conditions near 295 K without OH scavenger and seed particles added. The initial experimental conditions and results are listed in Table 6. Initial mixing ratios of α-pinene varied from 13 to 87 ppb. An aerosol density of 1 g cm^{-3} was assumed to convert the volume concentration into the mass concentration for the calculation of aerosol yields. Comparison of yield data of this work and previous studies (Hoffmann et al., 1997; Griffin et al., 1999; Cocker et al., 2001b; Saathoff et al., 2009; Wang et al., 2011) is shown in Fig. 7. The two-product model gives a good fit for the yield data obtained in this work. The appropriate values for α_1, α_2, $K_{om,1}$, $K_{om,2}$ are 0.189, 0.486, 0.0958, 0.00218, respectively. Only the data of Saathoff et al. (2009) are slightly higher than the yield curve obtained in this work, probably for they assumed an aerosol density of 1.25 g cm^{-3} when calculating aerosol mass concentrations. Most yield data of other studies are lower than the yields in this work for the same amount of SOA generated. This may be attributed to the influence of temperature because SOA yield is demonstrated to inversely depend on temperature (Saathoff et al., 2009).

4   Conclusions

We have built an indoor smog chamber ever largest in China, and initial characterization experiments described in this paper demonstrate that our GIG-CAS smog chamber facility can be used to provide valuable data for gas-phase mechanisms and aerosol chemistry. The chamber is shown to exhibit good temperature homogeneity and mixing efficiency. Observed relative lower wall loss rates of gas species and particles reflect long lifetime of these species and small wall effects. Results of propene-NO_x-air irradiation experiments illustrate its utility for evaluating gas phase chemical mechanisms. Furthermore, the good reproducibility of α-pinene ozonolysis experiments and good agreement with previous studies demonstrate its ability to study secondary organic aerosol formation.

References

Akimoto, H., Hoshino, M., Inoue, G., Sakamaki, F., Washida, N., and Okuda, M.: Design and characterization of the evacuable and bakable photochemical smog chamber, Environ. Sci. Technol., 13, 471–475, doi:10.1021/es60152a014, 1979.

Atkinson, R., Baulch, D. L., Cox, R. A., Crowley, J. N., Hampson, R. F., Hynes, R. G., Jenkin, M. E., Rossi, M. J., and Troe, J.: Evaluated kinetic and photochemical data for atmospheric chemistry: Volume I – gas phase reactions of O_x, HO_x, NO_x and SO_x species, Atmos. Chem. Phys., 4, 1461–1738, doi:10.5194/acp-4-1461-2004, 2004.

Bloss, C., Wagner, V., Jenkin, M. E., Volkamer, R., Bloss, W. J., Lee, J. D., Heard, D. E., Wirtz, K., Martin-Reviejo, M., Rea, G., Wenger, J. C., and Pilling, M. J.: Development of a

detailed chemical mechanism (MCMv3.1) for the atmospheric oxidation of aromatic hydro-carbons, Atmos. Chem. Phys., 5, 641–664, doi:10.5194/acp-5-641-2005, 2005.

Carter, W. P. L.: Documentation of the SAPRC-99 Chemical Mechanism for VOC Reactivity Assessment, Report to the California Air Resources Board, Contracts 92–329 and 95–308, 8 May 2000, 2000.

Carter, W. P. L. and Lurmann, F. W.: Evaluation of a detailed gas-phase atmospheric reaction mechanism using environmental chamber data, Atmos. Environ. A-Gen., 25, 2771–2806, doi:10.1016/0960-1686(91)90206-M, 1991.

Carter, W. P. L., Atkinson, R., Winer, A. M., and Pitts, J. N.: Experimental investigation of chamber-dependent radical sources, Int. J. Chem. Kinet., 14, 1071–1103, doi:10.1002/kin.550141003, 1982.

Carter, W. P. L., Luo, D., Malkina, I. L., and Pierce, J. A.: Environmental chamber studies of atmospheric reactivities of Volatile Organic Compounds: effects of varying chamber and light source, California Air Resources Board, 1995.

Carter, W. P. L., Cocker, D. R., Fitz, D. R., Malkina, I. L., Bumiller, K., Sauer, C. G., Pisano, J. T., Bufalino, C., and Song, C.: A new environmental chamber for evaluation of gas-phase chemical mechanisms and secondary aerosol formation, Atmos. Environ., 39, 7768–7788, doi:10.1016/j.atmosenv.2005.08.040, 2005.

Chan, C. K. and Yao, X. H.: Air pollution in mega cities in China, Atmos. Environ., 42, 1–42, 2008.

Cocker, D. R., Flagan, R. C., and Seinfeld, J. H.: State-of-the-art chamber facility for studying atmospheric aerosol chemistry, Environ. Sci. Technol., 35, 2594–2601, doi:10.1021/Es0019169, 2001a.

Cocker, D. R., Clegg, S. L., Flagan, R. C., and Seinfeld, J. H.: The effect of water on gas–particle partitioning of secondary organic aerosol. Part I: α-pinene/ozone system, Atmos. Environ., 35, 6049–6072, doi:10.1016/S1352-2310(01)00404-6, 2001b.

DeCarlo, P. F., Kimmel, J. R., Trimborn, A., Northway, M. J., Jayne, J. T., Aiken, A. C., Gonin, M., Fuhrer, K., Horvath, T., Docherty, K. S., Worsnop, D. R., and Jimenez, J. L.: Field-deployable, high-resolution, time-of-flight aerosol mass spectrometer, Anal. Chem., 78, 8281–8289, doi:10.1021/ac061249n, 2006.

Dodge, M. C.: Chemical oxidant mechanisms for air quality modeling: critical review, Atmos. Environ., 34, 2103–2130, doi:10.1016/S1352-2310(99)00461-6, 2000.

Title Page

Abstract | Introduction

Conclusions | References

Tables | Figures

|◄ | ►|

◄ | ►

Back | Close

Full Screen / Esc

Printer-friendly Version

Interactive Discussion

Donahue, N. M., Henry, K. M., Mentel, T. F., Kiendler-Scharr, A., Spindler, C., Bohn, B., Brauers, T., Dorn, H. P., Fuchs, H., Tillmann, R., Wahner, A., Saathoff, H., Naumann, K.-H., Möhler, O., Leisner, T., Müller, L., Reinnig, M.-C., Hoffmann, T., Salo, K., Hallquist, M., Frosch, M., Bilde, M., Tritscher, T., Barmet, P., Praplan, A. P., DeCarlo, P. F., Dommen, J., Prévôt, A. S. H., and Baltensperger, U.: Aging of biogenic secondary organic aerosol via gas-phase OH radical reactions, P. Natl. Acad. Sci., 109, 13503–13508, doi:10.1073/pnas.1115186109, 2012.

Griffin, R. J., Cocker III, D. R., Flagan, R. C., and Seinfeld, J. H.: Organic aerosol formation from the oxidation of biogenic hydrocarbons, J. Geophys. Res., 104, 3555–3567, doi:10.1029/1998jd100049, 1999.

Grosjean, D.: Wall loss of gaseous pollutants in outdoor Teflon chambers, Environ. Sci. Technol., 19, 1059–1065, doi:10.1021/es00141a006, 1985.

Hess, G. D., Carnovale, F., Cope, M. E., and Johnson, G. M.: The evaluation of some photochemical smog reaction mechanisms – I. Temperature and initial composition effects, Atmos. Environ. A-Gen., 26, 625–641, doi:10.1016/0960-1686(92)90174-J, 1992.

Hoffmann, T., Odum, J. R., Bowman, F., Collins, D., Klockow, D., Flagan, R. C., and Seinfeld, J. H.: Formation of organic aerosols from the oxidation of biogenic hydrocarbons, J. Atmos. Chem., 26, 189–222, 1997.

Hynes, R. G., Angove, D. E., Saunders, S. M., Haverd, V., and Azzi, M.: Evaluation of two MCM v3.1 alkene mechanisms using indoor environmental chamber data, Atmos. Environ., 39, 7251–7262, 2005.

Jayne, J. T., Leard, D. C., Zhang, X., Davidovits, P., Smith, K. A., Kolb, C. E., and Worsnop, D. R.: Development of an aerosol mass spectrometer for size and composition analysis of submicron particles, Aerosol. Sci. Tech., 33, 49–70, doi:10.1080/027868200410840, 2000.

Jeffries, H. E., Kamens, R. M., Sexton, K. G., and Gerhardt, A. A.: Outdoor Smog Chamber Experiments to Test Photochemical Models, EPA-600/3-82-016a, 1982.

Jeffries, H. E., Sexton, K. G., Kamens, R. M., and Holleman, M. S.: Outdoor Smog Chamber Experiments to Test Photochemical Models: Phase II, Final Report, EPA-600/3-85-029, 1985.

Johnson, D., Jenkin, M. E., Wirtz, K., and Martin-Reviejo, M.: Simulating the formation of secondary organic aerosol from the photooxidation of toluene, Environ. Chem., 1, 150–165, doi:10.1071/EN04069, 2004.

Jordan, A., Haidacher, S., Hanel, G., Hartungen, E., Mark, L., Seehauser, H., Schottkowsky, R., Sulzer, P., and Mark, T. D.: A high resolution and high sensitivity proton-transfer-reaction time-of-flight mass spectrometer (PTR-TOF-MS), Int. J. Mass Spectrom., 286, 122–128, 2009.

Leone, J. A., Flagan, R. C., Grosjean, D., and Seinfeld, J. H.: An outdoor smog chamber and modeling study of toluene-NO_x photooxidation, Int. J. Chem. Kinet., 17, 177–216, doi:10.1002/kin.550170206, 1985.

Lindinger, W., Hansel, A., and Jordan, A.: On-line monitoring of volatile organic compounds at pptv levels by means of proton-transfer-reaction mass spectrometry (PTR-MS) medical applications, food control and environmental research, Int. J. Mass Spectrom., 173, 191–241, 1998.

Martín-Reviejo, M. and Wirtz, K.: Is benzene a precursor for secondary organic aerosol?, Environ. Sci. Technol., 39, 1045–1054, doi:10.1021/es049802a, 2005.

Metzger, A., Dommen, J., Gaeggeler, K., Duplissy, J., Prevot, A. S. H., Kleffmann, J., Elshorbany, Y., Wisthaler, A., and Baltensperger, U.: Evaluation of 1,3,5 trimethylbenzene degradation in the detailed tropospheric chemistry mechanism, MCMv3.1, using environmental chamber data, Atmos. Chem. Phys., 8, 6453–6468, doi:10.5194/acp-8-6453-2008, 2008.

Odum, J. R., Hoffmann, T., Bowman, F., Collins, D., Flagan, R. C., and Seinfeld, J. H.: Gas/particle partitioning and secondary organic aerosol yields, Environ. Sci. Technol., 30, 2580–2585, doi:10.1021/es950943+, 1996.

Odum, J. R., Jungkamp, T. P. W., Griffin, R. J., Forstner, H. J. L., Flagan, R. C., and Seinfeld, J. H.: Aromatics, reformulated gasoline, and atmospheric organic aerosol formation, Environ. Sci. Technol., 31, 1890–1897, doi:10.1021/es960535l, 1997.

Pandis, S. N., Paulson, S. E., Seinfeld, J. H., and Flagan, R. C.: Aerosol formation in the photooxidation of isoprene and β-pinene, Atmos. Environ. A-Gen., 25, 997–1008, doi:10.1016/0960-1686(91)90141-S, 1991.

Paulsen, D., Dommen, J., Kalberer, M., Prévôt, A. S. H., Richter, R., Sax, M., Steinbacher, M., Weingartner, E., and Baltensperger, U.: Secondary organic aerosol formation by irradiation of 1,3,5-trimethylbenzene-NO_x-H_2O in a new reaction chamber for atmospheric chemistry and physics, Environ. Sci. Technol., 39, 2668–2678, doi:10.1021/es0489137, 2005.

Pinho, P. G., Pio, C. A., Carter, W. P. L., and Jenkin, M. E.: Evaluation of alkene degradation in the detailed tropospheric chemistry mechanism, MCM v3, using environmental chamber data, J. Atmos. Chem., 55, 55–79, doi:10.1007/s10874-006-9025-y, 2006.

Design and characterization of a smog chamber

X. Wang et al.

Title Page

Abstract | Introduction

Conclusions | References

Tables | Figures

|◄ | ►|

◄ | ►

Back | Close

Full Screen / Esc

Printer-friendly Version

Interactive Discussion

Ren, K., Li, J., Wang, W., and Zhang, H.: Investigation on experiment system for modeling of photochemical smog, Acta Scientiae Circumatantiae, 25, 1431–1435, 2005.

Rollins, A. W., Kiendler-Scharr, A., Fry, J. L., Brauers, T., Brown, S. S., Dorn, H.-P., Dubé, W. P., Fuchs, H., Mensah, A., Mentel, T. F., Rohrer, F., Tillmann, R., Wegener, R., Wooldridge, P. J., and Cohen, R. C.: Isoprene oxidation by nitrate radical: alkyl nitrate and secondary organic aerosol yields, Atmos. Chem. Phys., 9, 6685–6703, doi:10.5194/acp-9-6685-2009, 2009.

Saathoff, H., Naumann, K.-H., Möhler, O., Jonsson, Å. M., Hallquist, M., Kiendler-Scharr, A., Mentel, Th. F., Tillmann, R., and Schurath, U.: Temperature dependence of yields of secondary organic aerosols from the ozonolysis of α-pinene and limonene, Atmos. Chem. Phys., 9, 1551–1577, doi:10.5194/acp-9-1551-2009, 2009.

Saunders, S. M., Jenkin, M. E., Derwent, R. G., and Pilling, M. J.: Protocol for the development of the Master Chemical Mechanism, MCM v3 (Part A): tropospheric degradation of non-aromatic volatile organic compounds, Atmos. Chem. Phys., 3, 161–180, doi:10.5194/acp-3-161-2003, 2003.

Simonaitis, R., Meagher, J. F., and Bailey, E. M.: Evaluation of the condensed carbon bond (CB-IV) mechanism against smog chamber data at low VOC and NO_x concentrations, Atmos. Environ., 31, 27–43, doi:10.1016/S1352-2310(96)00155-0, 1997.

Stern, J. E., Flagan, R. C., Grosjean, D., and Seinfeld, J. H.: Aerosol formation and growth in atmospheric aromatic hydrocarbon photooxidation, Environ. Sci. Technol., 21, 1224–1231, doi:10.1021/es00165a011, 1987.

Sulzer, P. and Mark, T. D.: A high resolution and high sensitivity proton-transfer-reaction time-of-flight mass spectrometer (PTR-TOF-MS), Int. J. Mass Spectrom., 286, 122–128, 2009.

Tang, J. H., Wang, X. M., Feng, Y. L., Sheng, G. Y., and Fu, J. M.: Determination of C-1 similar to C-10 carbonyls in the atmosphere, Chinese J. Anal. Chem., 31, 1468–1472, 2003.

Vlasenko, A., Macdonald, A .M., Sjostedt, S. J., and Abbatt, J. P. D.: Formaldehyde measurements by Proton transfer reaction – Mass Spectrometry (PTR-MS): correction for humidity effects, Atmos. Meas. Tech., 3, 1055–1062, doi:10.5194/amt-3-1055-2010, 2010.

Wang, J., Doussin, J. F., Perrier, S., Perraudin, E., Katrib, Y., Pangui, E., and Picquet-Varrault, B.: Design of a new multi-phase experimental simulation chamber for atmospheric photosmog, aerosol and cloud chemistry research, Atmos. Meas. Tech., 4, 2465–2494, doi:10.5194/amt-4-2465-2011, 2011.

Wang, W., Xie, Y., Lin, Z., and Wang, H.: Study on reaction rate constants of CH_4 and its lifetime, China Enviromental Science, 15, 258–261, 1995.

Design and characterization of a smog chamber

X. Wang et al.

Title Page

Abstract	Introduction
Conclusions	References
Tables	Figures

|◄ | ►|

◄ | ►

| Back | Close |

Full Screen / Esc

Printer-friendly Version

Interactive Discussion

Wang, X. M. and Wu. T.: Release of isoprene and monoterpenes during the aerobic decomposition of orange wastes from laboratory incubation experiments, Environ. Sci. Technol., 42, 3265–3270, 2008.

Wu, S., Lü, Z., Hao, J., Zhao, Z., Li, J., Takekawa, H., Minoura, H., and Yasuda, A.: Construction and characterization of an atmospheric simulation smog chamber, Adv. Atmos. Sci., 24, 250–258, doi:10.1007/s00376-007-0250-3, 2007.

Xu, Y., Jia, L., Ge, M., Du, L., Wang, G., and Wang, D.: A kinetic study of the reaction of ozone with ethylene in a smog chamber under atmospheric conditions, Chinese Sci. Bull., 51, 2839–2843, doi:10.1007/s11434-006-2180-3, 2006.

Zhang, Q., He, K. B., and Huo, H.: Clean China's air, Nature, 484, 161–162, 2012.

Zhang, Y. L., Guo, H., Wang, X. M., Simpson, I. J., Barletta, B., Blake, D. R., Meinardi, S., Rowland, F. S., Cheng, H. R., Saunders, S. M., and Lam, S. H. M.: Emission patterns and spatiotemporal variations of halocarbons in the Pearl River Delta region, Southern China, J. Geophys. Res.-Atmos., 115, D15309, doi:10.1029/2009JD013726, 2010.

Zhang, Y. L., Wang, X. M., Blake, D. R., Li, L. F., Zhang, Z., Wang, S. Y., Guo, H., Lee, F. S. C., Gao, B., Chan, L. Y., Wu, D., and Rowland, F. S.: Aromatic hydrocarbons as ozone precursors before and after outbreak of the 2008 financial crisis in the Pearl River Delta region, South China, J. Geophys. Res.-Atmos., 117, D15306, doi:10.1029/2011JD017356, 2012.

Zhang, Y., Wang, X., Zhang, Z., Lü, S., Shao, M., Lee, F. S. C., and Yu, J.: Species profiles and normalized reactivity of volatile organic compounds from gasoline evaporation in China, Atmos. Environ., 79, 110–118, doi:10.1016/j.atmosenv.2013.06.029, 2013.

Title Page

Abstract | Introduction

Conclusions | References

Tables | Figures

◄ | ►

◄ | ►

Back | Close

Full Screen / Esc

Printer-friendly Version

Interactive Discussion

Table 1. Overview of instruments.

Instrument	Measured parameters	DL/Range	Accuracy	Flow rate ($L\,min^{-1}$)
Siemens QFM2160	temperature	0–50 °C or −35–35 °C	±0.8 °C	NA[a]
	relative humidity	0–100 %	±3 %	NA
Siemens QBM66.201	differential pressure	0–100 Pa	±3 Pa	NA
EPP2000CXR-50 Concave Grating spectrometer	light spectrum	280–900 nm	NA	NA
Thermo ScientificModel 48i	CO	0.04 ppm	±0.1 ppm	0.5
Thermo Scientific Model 43i	SO_2	0.05 ppb	0.2 ppb or ±1 %[b]	0.5
Ecotech 9810	O_3	0.5 ppb	0.5 ppb or ±0.5 %[b]	0.5
Ecotech 9841T	$NO/NO_2/NO_x$	50 ppt	100 ppt or ±0.5 %[b]	0.64
Ecotech 9842	NO_x/NH_3	0.5 ppb	±0.5 %	0.355
GC-MSD/FID/ECD	VOCs	< 10 ppt	±5 %	NA
PTR-TOF-MS	VOCs	0.1–5000 ppb	±(5–30) %	0.5
DNPH-LC-MS	carbonyls	0.05–0.15 $\mu g\,m^{-3}$	±3 %	NA
SMPS (TSI 3081DMA and 3775 CPC)	particle number	1–10^7 cm^{-3}	±10 %[c]	0.3
	particle size	10–1000 nm	±(3–3.5) %	
HR-TOF-AMS	particle composition	NA	NA	1.0

[a] NA = not applicable.
[b] Whichever is greater.
[c] For total number concentration.

Table 2. Summary of wall loss rates of gas species in GIG-CAS chamber and comparison with other chamber facilities.

Species	Run numbers	Temp (K)	RH (%)	Wall loss rate ($\times 10^{-4}\,\mathrm{min}^{-1}$)			
				GIG-CAS (30 m^3)	ERT[a] (60 m^3)	EUPHORE[b] (200 m^3)	PSI[c] (27 m^3)
O_3	4	296.7	< 10	1.31 ± 0.24	$0.5 \sim 3$	1.8	2.4
NO	9	296.7	< 10	1.41 ± 0.40	$0 \sim 5.4$	NA[d]	NA
NO_2	4	296.7	< 10	1.39 ± 0.68	$0 \sim 2$	NA	$0.13 \sim 2.52$

[a] Grosjean. (1985).
[b] Bloss et al. (2005).
[c] Metzger et al. (2008).
[d] NA = not applicable.

Table 3. Comparison of particle wall loss rates in different smog chambers.

chamber	volume (m^3)	wall material	wall loss rate (h^{-1})	particle lifetime (h)	Reference
GIG-CAS	3	FEP	0.17	5.9	This work
PSI	27	FEP	0.21	4.8	Paulsen et al. (2005)
Caltech	28	FEP	0.20	5	Cocker et al. (2001a)
UCR	90	FEP	0.29	3.4	Carter et al. (2005)
EUPHORE	200	FEP	0.18	5.6	Martin-Reviejoet and Wirtz (2005)
SAPHIR	270	FEP	0.27	3.7	Rollins et al. (2009)
CMU	12	FEP	0.40	2.5	Donahue et al. (2012)

Title Page

Abstract | Introduction

Conclusions | References

Tables | Figures

|◄ | ►|

◄ | ►

Back | Close

Full Screen / Esc

Printer-friendly Version

Interactive Discussion

Table 4. Summary of initial conditions for propene-NO_x-air irradiation experiments.

Run number	T(K)	RH %	J_{NO_2} min^{-1}	[propene]$_0$ ppb	[NO]$_0$ ppb	[NO$_2$]$_0$ ppb	[propene]/[NO$_x$]
1	298.2 ± 0.5	< 10	0.49	878	215	126	2.6
2	298.2 ± 0.3	< 10	0.49	967	132	292	2.3
3	297.9 ± 0.3	< 10	0.34	930	447	2.6	2.1
4	299.0 ± 0.8	< 10	0.49	669	350	19	1.8

Table 5. Auxiliary mechanisms for chamber-dependent reactions.

Reaction	Parameters	Lower/Upper limits
$h\nu \xrightarrow{\text{wall}} NO_2$	$0.005 J_{NO_2}\,\mathrm{ppbv\,s^{-1}}$	$(0.0025 \sim 0.010) J_{NO_2}\,\mathrm{ppbv\,s^{-1}}$
$h\nu \xrightarrow{\text{wall}} OH$	$0.005 J_{NO_2}\,\mathrm{ppbv\,s^{-1}}$	$(0.0025 \sim 0.010) J_{NO_2}\,\mathrm{ppbv\,s^{-1}}$
$NO_2 \rightarrow 0.5HONO + wHNO_3$ [a]	$2.31 \times 10^{-6}\,\mathrm{s^{-1}}$	$(1.17 \sim 3.45) \times 10^{-6}\,\mathrm{s^{-1}}$
$N_2O_5 \longrightarrow 2wHNO_3$	$1 \times 10^{-5}\,\mathrm{s^{-1}}$	$(0.5 \sim 2.0) \times 10^{-6}\,\mathrm{s^{-1}}$
$N_2O_5 + H_2O \longrightarrow 2wHNO_3$	$1 \times 10^{-20}\,\mathrm{cm^3\,molecule^{-1}\,s^{-1}}$	$(0.1 \sim 10) \times 10^{-20}\,\mathrm{cm^3\,molecule^{-1}\,s^{-1}}$
$wHNO_3 \xrightarrow{h\nu} OH + NO_2$	J_{HNO_3}	$(0.5 \sim 2.0) J_{HNO_3}$
$HNO_3 \rightarrow wHNO_3$	$1 \times 10^{-4}\,\mathrm{s^{-1}}$	$(0.5 \sim 2.0) \times 10^{-4}\,\mathrm{s^{-1}}$
$NO \longrightarrow wNO$	$2.34 \times 10^{-6}\,\mathrm{s^{-1}}$	$(1.68 \sim 3.00) \times 10^{-6}\,\mathrm{s^{-1}}$
$O_3 \longrightarrow wO_3$	$2.19 \times 10^{-6}\,\mathrm{s^{-1}}$	$(1.79 \sim 2.59) \times 10^{-6}\,\mathrm{s^{-1}}$
$[HONO]_0$	Varied from $0 \sim 5\,\mathrm{ppb}$	

[a] $wHNO_3$ represents adsorbed HNO_3 on the wall, similarly, wNO and wO_3 represent adsorbed NO and O_3, respectively.

Table 6. Summary of initial conditions and results for α-pinene ozonolysis experiments.

Run number	T(K)	RH (%)	[α-pinene] ppb	[O_3] ppb	ΔROG $\mu g\,m^{-3}$	M_0 $\mu g\,m^{-3}$	Y
1	296 ± 0.4	< 5	69.7	179	390.9	114.2	0.292
2	295 ± 0.6	< 5	21.8	425	122.4	23.9	0.195
3	294 ± 0.5	< 5	87.2	435	492.4	190.8	0.387
4	292 ± 1.8	< 5	34.7	806	196.8	45.1	0.229
5	292 ± 0.7	< 5	13.1	626	74.2	4.98	0.067
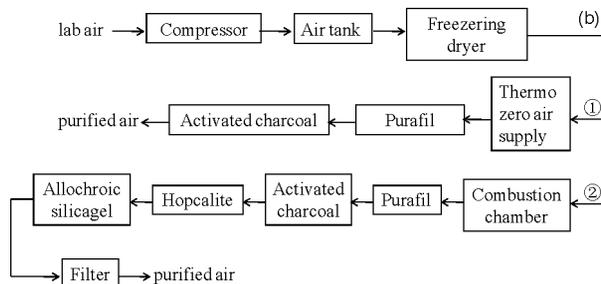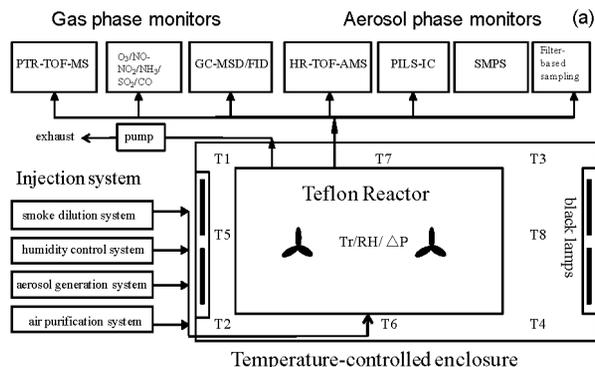
Fig. 1. (a) Schematic of the GIG-CAS smog chamber facility. T_1-T_8 are thermocouples in the enclosure and T_r is temperature sensor inside the reactor. **(b)** Schematic of two air purification systems. Route 1 represents the procedures of the Thermo zero air supply system; Route 2 represents the procedures of the larger flow rate air purification system.

Title Page

Abstract | Introduction

Conclusions | References

Tables | Figures

|◄ | ►|

◄ | ►

Back | Close

Full Screen / Esc

Printer-friendly Version

Interactive Discussion
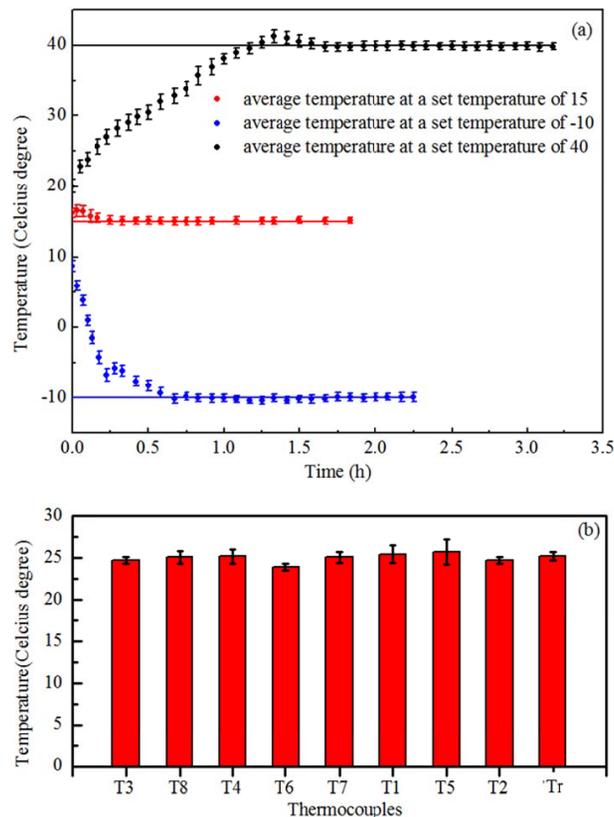
Fig. 2. (a) Evolutions of the average temperature of nine thermocouples, eight of them outside the reactor and one inside the reactor (see Fig. 1a), under black light irradiation condition. Error bars are the standard deviations of the nine temperatures. The solid lines represent set temperatures. **(b)** Average temperature values measured by thenine thermocouples over a 6 h period under black light irradiation condition. Error bars show the temperature variability in the 6 h period.
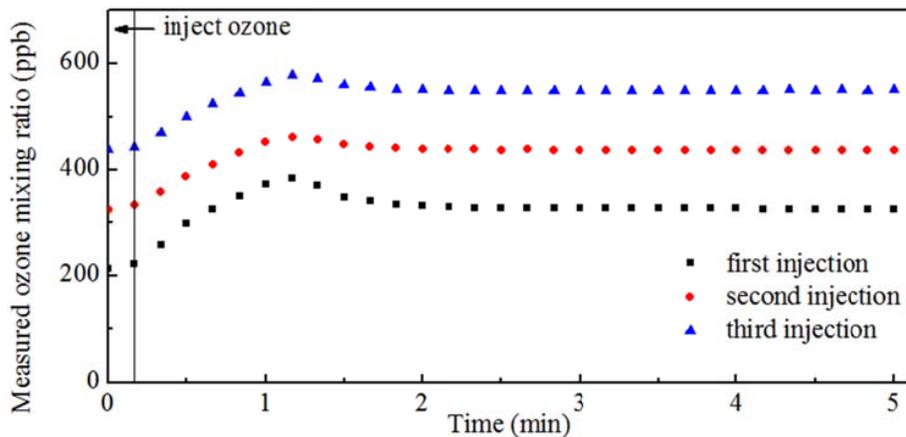
Fig. 3. Concentration-time plot of ozone after each injection.The two mixing fans rotated at a speed of 700 rpm in the experiments.
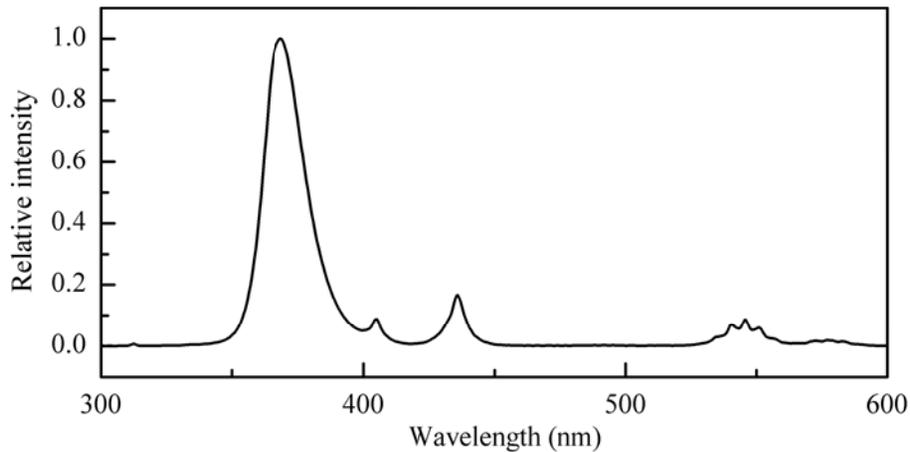
Fig. 4. Measured spectrum of black lamps.

Discussion Paper | Discussion Paper | Discussion Paper | Discussion Paper

AMTD

6, 7735–7769, 2013

Design and characterization of a smog chamber

X. Wang et al.

Title Page

Abstract | Introduction

Conclusions | References

Tables | Figures

|◄ | ►|

◄ | ►

Back | Close

Full Screen / Esc

Printer-friendly Version

Interactive Discussion
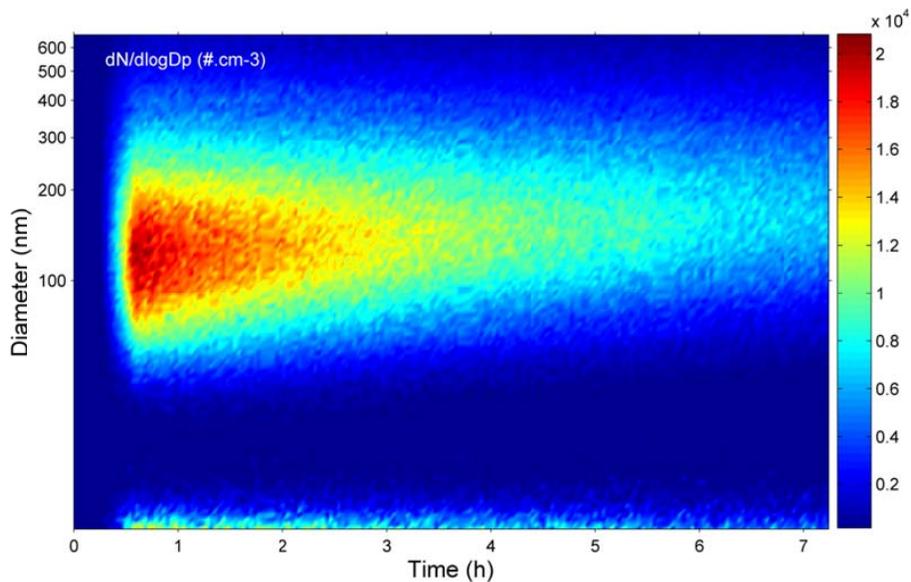
Fig. 5. Number concentration distribution of $(NH_4)_2SO_4$ as a function of time after its introduction into the reactor.
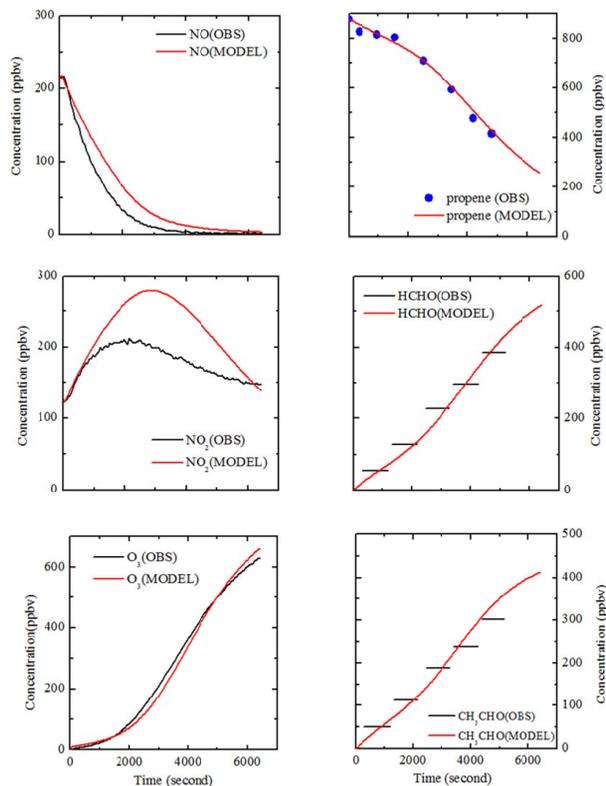
Fig. 6. Concentration-time plots of observed and simulated NO, NO_2, O_3, propene, HCHO and CH_3CHO in a propene-NO_x-air irradiation system.

Fig. 7. Comparison of yield data obtained for α-pinene ozonolysis experiments in GIG-CAS chamber with other chamber facilities. All experiments are carried out under dry condition. Blue line is the best fit two-product model for the data set of GIG-CAS.